Liquid Crystals
Publication details, including instructions for authors and subscription information:
http://www.informaworld.com/smpp/title~content=t713926090

Single-step exposure for two-dimensional electrically-tuneable diffraction grating based on polymer dispersed liquid crystal

Zhigang Zheng[ab]; Jing Song[c]; Yonggang Liu[a]; Fuzhong Guo[ab]; Ji Ma[d]; Li Xuan[a]
[a] State Key Laboratory of Applied Optics, Changchun Institute of Optics, Fine Mechanics and Physics, Chinese Academy of Science, Changchun 130033, China [b] Graduate School of Chinese Academy of Science, Beijing 100039, China [c] Materials Sciences and Engineering School, Changchun University of Sciences and Technology, Changchun 130022, China [d] Liquid Crystal Institute, Kent State University, Kent, OH 44240, USA

To cite this Article Zheng, Zhigang , Song, Jing , Liu, Yonggang , Guo, Fuzhong , Ma, Ji and Xuan, Li(2008) 'Single-step exposure for two-dimensional electrically-tuneable diffraction grating based on polymer dispersed liquid crystal', Liquid Crystals, 35: 4, 489 — 499
To link to this Article: DOI: 10.1080/02678290801956339
URL: http://dx.doi.org/10.1080/02678290801956339

Liquid Crystals,
Vol. 35, No. 4, April 2008, 489–499

Taylor & Francis
Taylor & Francis Group

Single-step exposure for two-dimensional electrically-tuneable diffraction grating based on polymer dispersed liquid crystal

Zhigang Zheng[ab]*, Jing Song[c], Yonggang Liu[a], Fuzhong Guo[ab], Ji Ma[d] and Li Xuan[a]

[a]*State Key Laboratory of Applied Optics, Changchun Institute of Optics, Fine Mechanics and Physics, Chinese Academy of Science, Changchun 130033, China;* [b]*Graduate School of Chinese Academy of Science, Beijing 100039, China;* [c]*Materials Sciences and Engineering School, Changchun University of Sciences and Technology, Changchun 130022, China;* [d]*Liquid Crystal Institute, Kent State University, Kent, OH 44240, USA*

(Received 13 November 2007; final form 30 January 2008)

The two-dimensional (2D) electrically tuneable grating exhibits a bright future in the fields of optics and communication. A 2D grating based on a polymer-dispersed liquid crystal (PDLC) with good electro-optical (E-O) properties was fabricated through a single-step exposure method. The E-O behaviour was measured and the morphology of the grating observed using polarising optical microscopy (POM) and atom force microscopy (AFM). In addition, a 2D diffraction model and photopolymerisation dynamics model are presented to evaluate the E-O properties and morphology of the grating. All results obtained from the model show good agreement with experimental data. These results indicate that the morphologies are fairly good when the intensity ratio of pair L and pair K, labelled in the experimental setup, was 1:1.

Keywords: polymer-dispersed liquid crystal; electrically-tuneable grating; liquid crystal diffraction efficiency

1. Introduction

The electrically tuneable polymer-dispersed liquid crystal (PDLC) grating is a new type of active optical device, which is fabricated by holographic exposure based on homogeneous pre-polymer mixed with photosensitive monomers and LCs (*1–5*). Because of its electrically-tuneable property, this kind of grating has already shown great prospects in the fields of reflective displays, light valves, zoom lens and telecommunications fields (*3–9*). The conventional electrically tuneable PDLC grating, which was proposed by Sutherland and co-workers, was prepared by means of two-beam interference and one-dimensional grating was recorded on the sample. One merit of such grating is that the intensity of diffraction beam could be modulated by a certain voltage. In order to widen the application of PDLC gratings, Bowley and Crawford prepared a multiplexed holographic grating through multi-beam interference (*10–12*). The success in multiplexed grating promotes the development of PDLC devices, especially in multi-path optical interconnection, multi-switch and massive information storage.

Recently, most researchers have focused on the fabrication of two-dimensional (2D) electrically-tuneable diffraction grating on PDLC film (*13–25*). The 2D diffraction grating is different from the multiplexed grating mentioned above. The vectors of every grating recorded in the sample are crossed with a certain angle in the former, whereas they are parallel with each other in the latter. The 2D grating can diffract incident light in various directions. It can be widely applied in optical beam steering, beam splitters or phase modulation devices (*13, 16–20*). At present, the methods that have been adopted to prepare a 2D PDLC grating are as follows: (1) covering a photomask with a 2D structure on the sample and curing with UV or laser (*13–15*); (2) putting the acute prisms or the flat-topped pyramids at the front of the sample, the incidence beam is divided by multi-beams and these beams converge at equal angles, and form the 2D interference pattern, which is recorded on the surface of the sample (*21–24*). In addition, other intricate techniques have also been used. For example, Ma *et al.* (*25*) adopted double exposure with a two-beam interference field to prepare a 2D grating. They exposed their sample for 20 s initially, then rotated it about 90° and exposed it again for 3 min to form the 2D grating. These methods are suitable for the preparation of 2D gratings, but they have some inherent shortcomings. Photomask exposure is very convenient, but the patterns of the hologram are restricted by the mask. Therefore, one mask corresponds to one hologram. The prisms or pyramids can control the relative phase of the multi-beams easily; however, they bring more reflecting surfaces into the optical path, which greatly affects the laser beam quality. Also, the period of the 2D structure is dependent on the apex angle of the prism; thus it is very inconvenient to prepare gratings

*Corresponding author. Email: zhigang1982@sina.com

ISSN 0267-8292 print/ISSN 1366-5855 online

DOI: 10.1080/02678290801956339
http://www.informaworld.com

with different periods. Double exposure is more complicated, although the method can modulate the period of the grating.

In this paper, a single-step exposure method is presented for the formation of a 2D electrically-tuneable diffraction grating based on a PDLC. Compared with previous techniques, the method is more convenient and the period of the grating can be varied arbitrarily. In addition, four mirrors are used to substitute the prism, which will decrease the reflecting surface and improve beam quality. The materials used and the experimental setup are described in section 2. Two detailed theoretical studies of such a 2D grating are reported. In section 3.1, the diffraction intensity distributions are simulated through scalar diffraction theory in the cases of no applied voltage and an applied voltage of $12.5\,\mathrm{V\,\mu m^{-1}}$. In section 3.2, a 2D photopolymerisation dynamics model is developed to express the morphologies of the grating under different exposure conditions. The results obtained from theoretical simulation are listed and discussed in section 4. All of them show good agreement with our experiment and lead to more improvements of 2D switchable PDLC gratings. Finally, the conclusions are given in section 5.

2. Experiments

Materials and sample preparation

In the experiment, the prepolymer mainly consisted of two kinds of acrylate monomers, one a difunctional neopentyl glycol diacrylate (NPGDA) and the other a pentafunctional dipentaerythritol hydroxyl penta-acrylate (DPHPA), both of which were supplied by Aldrich. Blends of NPGDA and DPHPA had a ratio of 1:1 by weight. The nematic LC used in the experiment was TEB30A (Δn=0.1703 n_e=1.6925 at 20°C, Slichem Co. Ltd.). The weight ratio between prepolymer and LC was 7:3. A small amount of Rose Bengal (RB, Aldrich, 0.5 wt%) and *N*-phenylglycine (NPG, Aldrich, 2 wt%) were added in the mixture as photoinitiator and co-initiator, respectively. In addition, a type of fluorinated acrylate monomer, Actyflon-G04 (XEOGIA Fluorine-Silicon Chem. Co. Ltd.), was also added as the surfactant to decrease threshold voltage of 2D grating. These components were stirred at 35°C for 12 h, then injected in a glass cell with indium tin oxide (ITO) coated on the inner surface. The cell gap was 10 μm.

Experimental setup and testing

Two linear-polarised laser beams, the polarisation directions of which were vertical to each other, were generated by a polarisation beam splitter (PBS) placed behind the beam expander. The polarisation directions of the beams are labelled by two green double-arrows in Figure 1. The two beams were divided by two beam splitters, BS1 and BS2, to generate two pairs of beams (labelled pair L and pair K in Figure 1). Thus, the problem of phase difference between the two pairs of beams is irrelevant. One pair of them (labelled L1 and L2) radiates on the sample

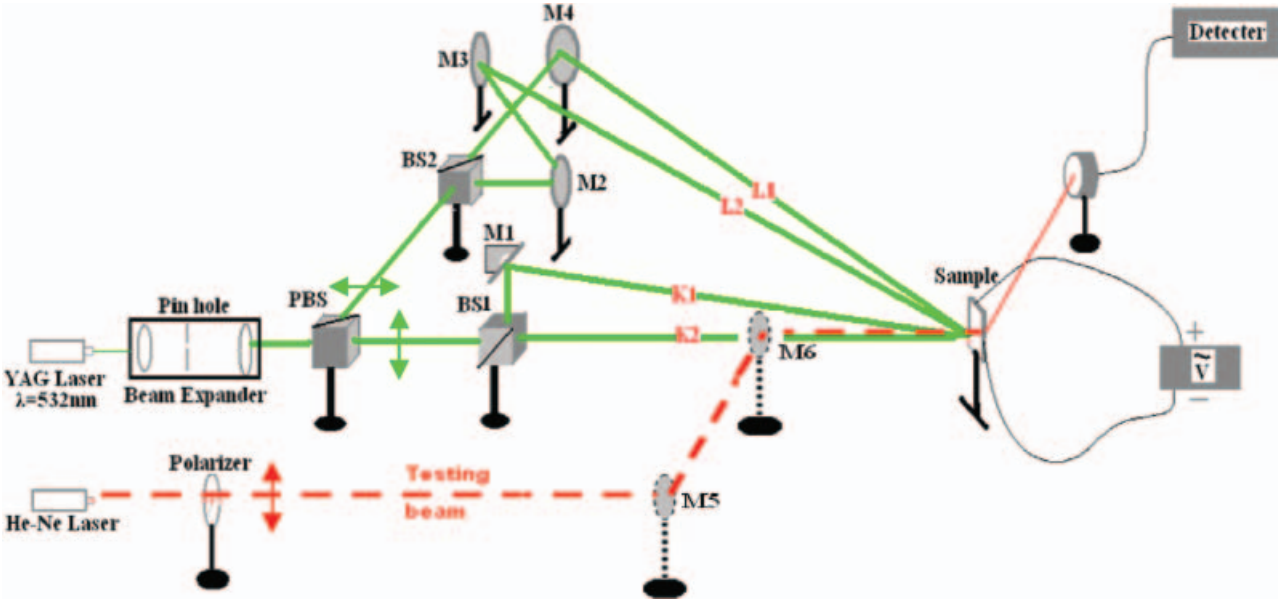

Figure 1. Experimental and testing setup: the green solid line is the single-step exposure setup, and the red dashed line denotes the testing laser and the elements used in E-O testing only. The green double-arrows represent the polarisation direction of two pairs of recording beams, and the red double-arrow represents the polarisation direction of testing beam.

at an angle of about 3°, forming longitudinal interference strips. The other (labelled K1 and K2) with the same angle, forms transverse strips overlapped at the same place of the sample. The intensity of each beam was 1.05 mW cm^{-2}, and the sample was exposed for about 20 min. Because of the vertical polarisation direction between pair L and pair K, there is no interference between L1 and K1, L1 and K2, L2 and K1 or L2 and K2. Thus, an ordered micro-square lattice array is recorded, and a 2D diffraction grating is obtained.

A He–Ne laser was utilised to test the diffraction characteristics and electrically switchable properties of the grating. The morphology of the grating was observed by polarising optical microscopy (POM, Olympus BX51) and atom force microscopy (AFM, Dimension 3100). Before AFM testing, the sample was immersed in alcohol for about 24 h to extract the LCs, and then the sample placed on a slick slice and blow-dred with pure nitrogen, using the tapping mode to scan the sample, and detailed morphology pictures were obtained.

3. Theory

Diffractive distribution model of 2D grating based on PDLC

Similar to the conventional grating based on a PDLC, the 2D grating obtained through single-step exposure shows remarkable electro-optical (E-O) properties. When there is no applied voltage on the ITO electrodes, an incoming beam is diffracted by the grating and many diffraction orders can be observed in the 2D plane. This is called the "OFF" state. When the applied voltage exceeds a threshold (defined as the lowest voltage applied to the sample to change the orientation of LCs in the grating), the transmittance increases significantly, whereas the diffraction orders disappear gradually because of the reorientation of LCs, which leads to the refractive index difference between polymer and LC domain being close to zero. This is called the "ON" state.

There have been many theoretical reports about the E-O response of LCs. However, the theory of 2D PDLC gratings has rarely been reported. To explain the E-O behaviour of a 2D PDLC grating theoretically, a 2D diffraction model is established. Scalar diffraction theory is utilised to calculate the diffractive distribution, because the period of grating is much larger than the emitting wavelength (about 20 times larger) (*26*). Moreover, the voltage applied to the ITO electrodes is considered in the model.

Intensity distribution of 2D interference field.

Assume that the amplitudes of the four laser beams are approximately equal, and that the phase differences of L1, L2 and K1, K2 are zero. Thus, the interference field formed by pair L (L1 and L2) can be expressed as

$$I_x = 2A_0^2\left\{1+\cos\left[\frac{2\pi}{\Lambda}(\sin\theta_{\mathrm{L2}}-\sin\theta_{\mathrm{L1}})x\right]\right\}. \quad (1)$$

Similar to equation (1), the expression for the interference field caused by pair K (K1 and K2) is

$$I_y = 2A_0^2\left\{1+\cos\left[\frac{2\pi}{\Lambda}(\sin\theta_{\mathrm{K2}}-\sin\theta_{\mathrm{K1}})y\right]\right\}, \quad (2)$$

where A_0 is amplitude of every beam, θ_{L1} (θ_{L2}) is the angle between L1 (L2) and the optical axis, and θ_{K1} (θ_{K2}) is the angle between K1 (K2) and the optical axis and λ is the wavelength.

As is mentioned in section 2.2, there is no interference between pair L and K, so the intensity distribution on the surface of sample can be simply expressed as

$$\begin{aligned} I &= I_x + I_y \\ &= 2A_0^2\left\{2+\cos\left[\frac{2\pi}{\Lambda}(\sin\theta_{L2}-\sin\theta_{L1})x\right]\right. \\ &\quad \left.+\cos\left[\frac{2\pi}{\Lambda}(\sin\theta_{K2}-\sin\theta_{K1})y\right]\right\} \\ &= 2A_0^2\left(2+\cos\frac{2\pi}{\Lambda_x}x+\cos\frac{2\pi}{\Lambda_y}y\right), \end{aligned} \quad (3)$$

where Λ_x and Λ_y are periods of the 2D grating along the x (transverse) and y (longitudinal) directions, respectively. In the experiment, $\Lambda_x \approx \Lambda_y$.

Transmission function of 2D pure phase diffraction gratings

The transmission function of 2D pure phase gratings can be deduced according to following two assumptions. (1) The polymer thickness of the grating is proportional to the interference intensity of a certain area, and satisfies the following relation

$$d = t_0 I, \quad (4)$$

where d is polymer thickness, I is exposure intensity as expressed in equation (3) and t_0 is a coefficient. That is, the thickest polymer corresponds to the highest intensity. (2) At the highest interference intensity, the polymer thickness is equal to the cell

gap, d_0. Combine with equation (3), the following equation is obtained

$$8A_0^2 t_0 = d_0. \tag{5}$$

Thus, the phase of a beam transmit through the grating can be given as

$$\begin{aligned} \varphi &= A_1 - B_1\left[\sin\left(\frac{2\pi}{\Lambda_x}x\right) + \sin\left(\frac{2\pi}{\Lambda_y}y\right)\right] \\ A_1 &= \frac{kd_0}{2}(n_{\mathrm{LC}} + n_{\mathrm{P}}) \\ B_1 &= \frac{kd_0}{4}(n_{\mathrm{P}} - n_{\mathrm{LC}}), \end{aligned} \tag{6}$$

where n_{LC} and n_{P} are the refractive indexes of LCs and polymer, respectively, and k is the wavevector.

According to the transmission function of 1D pure phase grating, the 2D transmission function can be expressed as

$$t(x, y) = e^{i\varphi}\mathrm{rect}\left(\frac{x}{L_x}\right)\mathrm{rect}\left(\frac{y}{L_y}\right). \tag{7}$$

Substituting Equations (6) into (7) and omitting the term $\exp(iA_1)$, which has no effects on diffractive distribution, the transmission function for a 2D pure phase grating is

$$\begin{aligned} t(x, y) &= t(x)t(y) \\ &= \exp\left[i\frac{B_2}{2}\sin\left(\frac{2\pi}{\Lambda_x}x\right)\right]\mathrm{rect}\left(\frac{x}{L_x}\right) \\ &\quad \exp\left[i\frac{B_2}{2}\sin\left(\frac{2\pi}{\Lambda_y}y\right)\right]\mathrm{rect}\left(\frac{y}{L_y}\right), \end{aligned} \tag{8a}$$

$$B_2 = \frac{kd_0(n_{\mathrm{LC}} - n_p)}{2}, \tag{8b}$$

where B_2 is defined as the refractive index modulation of 2D grating and L_{x} and L_{y} are the macroscopic length and width of the grating prepared in the experiment.

Diffraction intensity distribution of 2D grating based on PDLC

In general, the intensity distribution of diffraction beams is calculated through a Fraunhofer diffraction integral. This method is very complex and the integral is rather difficult to calculate using a personal computer. In this model, a Fourier transform is adopted, in a way that is simpler and precise. Considering Equation (8a), the diffraction intensity distribution is given by

$$\begin{aligned} I_{diff} &= \{\mathrm{FT}^-[t(x, y)]\}^2 = \{\mathrm{FT}^-[t(x)]\}^2\{\mathrm{FT}^-[t(y)]\}^2 \\ &= \left\{\mathrm{FT}^-\left\{\exp\left[i\frac{B_2}{2}\sin\left(\frac{2\pi}{\Lambda_x}x\right)\right]\mathrm{rect}\left(\frac{x}{L_x}\right)\right\}\right\}^2 \\ &\quad \times \left\{\mathrm{FT}^-\left\{\exp\left[i\frac{B_2}{2}\sin\left(\frac{2\pi}{\Lambda_y}y\right)\right]\mathrm{rect}\left(\frac{y}{L_y}\right)\right\}\right\}^2, \end{aligned} \tag{9}$$

where FT^- represents the Fourier transform algorithm. The exponential terms contained in equation (9) can be expanded using Bessel identities.

$$\begin{aligned} \exp\left[i\frac{B_2}{2}\sin\left(\frac{2\pi}{\Lambda_x}x\right)\right] &= \sum_{m=-\infty}^{\infty} J_m\left(\frac{B_2}{2}\right)\exp\left(i\frac{2\pi}{\Lambda_x}mx\right) \\ \exp\left[i\frac{B_2}{2}\sin\left(\frac{2\pi}{\Lambda_y}y\right)\right] &= \sum_{n=-\infty}^{\infty} J_n\left(\frac{B_2}{2}\right)\exp\left(i\frac{2\pi}{\Lambda_y}ny\right), \end{aligned} \tag{10}$$

where m and n are Bessel orders.

Combining equation (9) and (10), we can obtain:

$$\begin{aligned} I_{diff} &= \left[(L_x \sin cL_x u) \otimes \sum_{m=-\infty}^{\infty} J_m\left(\frac{B_2}{2}\right)\delta\left(u - \frac{m}{\Lambda_x}\right)\right]^2 \times \\ &\quad \left[(L_y \sin cL_y v) \otimes \sum_{n=-\infty}^{\infty} J_n\left(\frac{B_2}{2}\right)\delta\left(v - \frac{n}{\Lambda_y}\right)\right]^2 \\ &= \sum_{m=-\infty}^{\infty} L_x^2 J_m^2\left(\frac{B_2}{2}\right)\sin c^2 L_x\left(u - \frac{m}{\Lambda_x}\right) \times \\ &\quad \sum_{n=-\infty}^{\infty} L_y^2 J_n^2\left(\frac{B_2}{2}\right)\sin c^2 L_y\left(v - \frac{n}{\Lambda_y}\right), \end{aligned} \tag{11}$$

where u and ν are coordinates on Fourier transform plane which corresponding to x and y of Cartesian coordinate, and u, ν can be calculated by following relations

$$u = \frac{x}{z},\ v = \frac{y}{z}. \tag{12}$$

In Equation (12), z represents the distance from the sample to the collecting screen. When the position of the screen is fixed, z is a constant. Then, the diffraction intensity distribution can be calculated according to following expression,

$$\begin{aligned} I(x, y, z) &= L_x^2 L_y^2 \sum_{m=-\infty}^{\infty} J_m^2\left(\frac{B_2}{2}\right)\left[\frac{\sin\frac{\pi}{\Lambda}L_x\left(\frac{x}{z} - \frac{m\lambda}{\Lambda_x}\right)}{\frac{\pi}{\Lambda}L_x\left(\frac{x}{z} - \frac{m\lambda}{\Lambda_x}\right)}\right]^2 \times \\ &\quad \sum_{n=-\infty}^{\infty} J_n^2\left(\frac{B_2}{2}\right)\left[\frac{\sin\frac{\pi}{\Lambda}L_y\left(\frac{y}{z} - \frac{n\lambda}{\Lambda_y}\right)}{\frac{\pi}{\Lambda}L_y\left(\frac{y}{z} - \frac{n\lambda}{\Lambda_y}\right)}\right]^2. \end{aligned} \tag{13}$$

Considering the reorientation of LC molecules caused by applied voltage on ITO electrodes of LC cell,which leads to the variation of refractive index modulation of the 2D PDLC grating, we need to reconsider the refractive index modulation B_2 contained in Equation (13).

Define n_{LC} as the refractive index of the LC. When there is a certain angle, θ, between the wavevector and LC direction, n_{LC} can expressed as

$$n_{LC} = \frac{n_o n_e}{\left(n_e^2 \cos^2\theta + n_o^2 \sin^2\theta\right)^{1/2}}, \tag{14}$$

where n_o and n_e are the ordinary refractive index and extraordinary refractive index of the LC, respectively.

The field-dependent equilibrium angle of the LC director is given by (*27*)

$$\theta(E) = \frac{1}{2}\tan^{-1}\left[\frac{\sin 2\theta_0}{\cos 2\theta_0 + (E/E_C)^2}\right], \tag{15}$$

where θ_0 is the angle between LC direction and the normal line of LC cell in the absence of an applied field and E_C is the critical switching field.

From Equations (8b) and (13)–(15), the electro-optical performance of 2D PDLC gratings can be obtained theoretically.

Two-dimensional photopolymerisation dynamic model for grating morphology

As mentioned in section 2.1, a small amount of photoinitiator RB and co-initiator NPG were contained in the materials recipe, which interact with each other and produce a large number of free radicals. This leads to photo-induced free-radical polymerisation (PIFP). The details of PIFP process are discussed below.

PIFP process.

The PIFP process is represented schematically by the following equations:

$$R_S + \hbar\omega \rightarrow R_{S^*}, \tag{16a}$$

$$R_{S^*} \rightarrow R_S + \hbar\omega', \tag{16b}$$

$$R_{S^*} \rightarrow R_{T^*}, \tag{16c}$$

$$R_{T^*} + C \rightarrow R^{\cdot -} + C^{\cdot} + H^+, \tag{16d}$$

$$C^{\cdot} + M \rightarrow CM^{\cdot}, \tag{16e}$$

$$CM^{\cdot} + (n-1)M \rightarrow C(M)_{n-1}M^{\cdot}. \tag{16f}$$

First, the photoinitiator RB absorbs laser energy $\hbar\omega$ and transits from the ground singlet state R_S to an excited singlet state R_{S^*}, as described by Equation (16a). Due to the instability of R_{S^*}, it can decay by fluorescence to the ground singlet state, as in Equation (16b), or undergoes a transition to an excited triplet state R_{T^*} through inter-system crossing, as in Equation (16c). R_{T^*} can undergo an electron transfer and interact with co-initiator C (in our material recipe, it is NPG), producing the primary free-radical $C^{\cdot}$, which can react with –C=C– contained in monomers to create many monomer free-radicals $CM^{\cdot}$. $CM^{\cdot}$ can react with other monomers continually, then, generate the chain free-radical $C(M)_{n-1}M^{\cdot}$, as in Equations (16d)–(16f). The chain free-radicals can react with other chain free-radicals or monomer free-radicals and lead to so called dead-end polymerisation or consume monomers and keep on extending.

Two-dimensional photopolymerisation dynamics model.

According to PIFP analysis, we consider the energy absorption of RB firstly. Through Lambert-Beer laws, and notice 2D interference intensity distribution expressed as Equation (3), assuming that the concentrations of R_S and R_{S^*} are represented by ϕ_s and ϕ_{s^*}, respectively, $\varepsilon(\lambda)$ is molar extinction coefficient of a certain radiated wavelength λ, l is thickness of materials and $\varepsilon(\lambda)\ \phi_s l$ is absorption caused by RB in materials. The energy absorbed is defined as I_a, and the generating rate of R_{S^*} is equals to I_a, we have,

$$\begin{aligned} I_a &= \frac{d\phi_{s^*}}{dt} = I\left(1 - 10^{-\varepsilon(\Lambda)\phi_S l}\right) \\ &= 2I_0\left(2 + \cos\frac{2\pi}{\Lambda_x}x + \cos\frac{2\pi}{\Lambda_y}y\right)\left(1 - 10^{-\varepsilon(\Lambda)\phi_S l}\right). \end{aligned} \tag{17}$$

In addition, ϕ_{s^*} is also obtained through equation (17):

$$\phi_{s^*} = 2I_0\left(2 + \cos\frac{2\pi}{\Lambda_x}x + \cos\frac{2\pi}{\Lambda_y}y\right)\left(1 - 10^{-\varepsilon(\Lambda)\phi_S l}\right)t. \tag{18}$$

where t is exposure time.

Since ϕ_{s^*} can be divided into two parts, i.e. decay by fluorescence (represented by ϕ_f) and interaction with NPG to create free radicals, which leads to photopolymerisation (represented by $\phi_{R_{T^*}}$), $\phi_{s^*} = \phi_{R_{T^*}} + \phi_f$. Define a triplet quantum yield, σ_T, which satisfies the equation $\sigma_T = \phi_{R_{T^*}}/\phi_{s^*}$. Thus, the

expression $\phi_{R_{T^*}}$ is obtained:

$$\phi_{R_{T^*}} = \sigma_T \times 2I_0 \left(2+\cos\frac{2\pi}{\Lambda_x}x+\cos\frac{2\pi}{\Lambda_y}y\right)\left(1-10^{-\varepsilon(\Lambda)\phi_S l}\right)t. \quad (19)$$

Combining Equations (16d) and (19), 1 a.u. R_{T^*} can interact with 1 a.u. co-initiator to generate 1 a.u. primary free radicals. Therefore, the concentration of primary free radicals ($\phi_{C^\cdot}$) is expressed as

$$\phi_{C^\cdot} = \sigma_T \times 2I_0 \left(2+\cos\frac{2\pi}{\Lambda_x}x+\cos\frac{2\pi}{\Lambda_y}y\right)\left(1-10^{-\varepsilon(\Lambda)\phi_S l}\right)t. \quad (20)$$

At the beginning of exposure, many free radicals are generated, and the time for generation is instantaneous, so this process can be considered a quasi-static state. Under quasi-static-state conditions, the generating rate of primary free radical is equal to that of chain free radicals (*28*). When the concentration of chain free radicals reaches equilibrium, we can consider that the generating rate and the consuming rate of chain free radical are equal each. Assuming that the free radicals are consumed by the way of dead-end polymerisation, the consuming rate can be expressed as $k_t\phi^2_{C(M)_{n-1}M^\cdot}$ (*29*). Thus, the following relation is obtained

$$\frac{\partial\phi_{C^\cdot}}{\partial t} = k_t\phi^2_{C(M)_{n-1}M^\cdot} = \sigma_T \times 2I_0 \left(2+\cos\frac{2\pi}{\Lambda_x}x+\cos\frac{2\pi}{\Lambda_y}y\right)\left(1-10^{-\varepsilon(\Lambda)\phi_S l}\right), \quad (21)$$

where $\phi^2_{C(M)_{n-1}M^\cdot}$ is the concentration of chain free radicals and k_t is the dead-end rate constant, which shows the speed of dead-end polymerisation.

In the whole process of photopolymerisation, the consuming rate of monomers is proportional to the monomer concentration and chain free-radical concentration in the reaction system and the proportional constant is k_P. The consumption rate of monomer is equal to the rate of polymer generation. Thus, following equation should be satisfied:

$$\frac{\partial\phi_M}{\partial t} = -k_P\phi_M\phi_{C(M)_{n-1}M^\cdot} = -\frac{\partial\phi_P}{\partial t}, \quad (22)$$

where ϕ_M and ϕ_P are the concentrations of monomer and polymer, respectively, in the reaction system and k_P is the polymerisation rate constant.

Let ϕ_{M0} be the monomer concentration before exposure. Combining Equations (21)–(22) and resolving differential Equation (22) under boundary conditions $\phi_M=\phi_{M0}$ when $t=0$ and $\phi_M=0$ when $t=\infty$, the concentration of polymer, ϕ_P, and the monomer conversion, $\alpha=\phi_P/\phi_{M0}$, are obtained:

$$\phi_P(x,y,t) = \phi_{M0}\left\{1-\exp\left[-\frac{k_P}{\sqrt{k_t}}t\sqrt{2I_0\sigma_T\left(2+\cos\frac{2\pi}{\Lambda_x}x+\cos\frac{2\pi}{\Lambda_y}y\right)(1-10^{-\varepsilon(\Lambda)\phi_s l})}\right]\right\}, \quad (23)$$

$$\alpha(x,y,t) = 1-\exp\left[-\frac{k_P}{\sqrt{k_t}}t\sqrt{2I_0\sigma_T\left(2+\cos\frac{2\pi}{\Lambda_x}x+\cos\frac{2\pi}{\Lambda_y}y\right)(1-10^{-\varepsilon(\Lambda)\phi_s l})}\right]. \quad (24)$$

4. Results and discussion

Morphology study

Andres Fernandez *et al.* have pointed out that there is a significant effect of phases between multi-beams on the interference structure (*30*). Apart from the phases, the more important effect comes from the

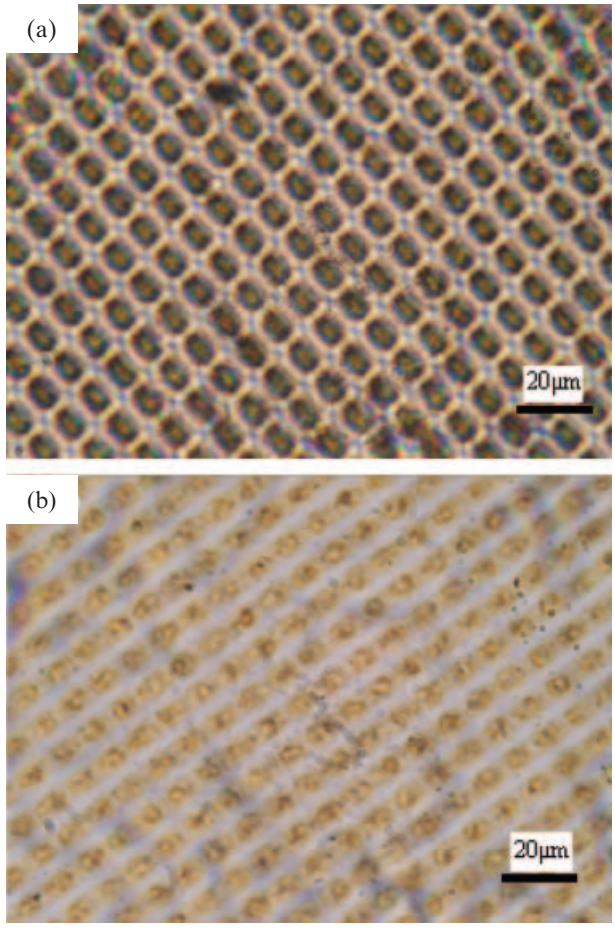

Figure 2. POM micrographs of samples prepared under conditions I_L/I_K=1:1 (a) and I_L/I_K=1:0.3 (b). Parallel polariser (1000×).

intensity of the beams. To describe this in detail, samples exposed under two exposure conditions (A: $I_L/I_K=1:1$; B: $I_L/I_K=1:0.3$) were prepared and their morphologies compared with each other from experiments and theoretical analysis. Figure 2 shows POM microphotographs of gratings prepared under the two conditions. The two photographs were obtained when the polarisers of the POM were parallel to each other. It can be seen that many more microsquare lattices are well-arranged and the outlines of the lattices are clear under condition A. In contrast, under condition B, the grating is almost one-dimensional and the outline is blurry.

Similar conclusions were also obtained by AFM also. Figures 3(a-1) and 3(b-1) show top-view images of the gratings. Under condition A, there are a lot of egg-shaped pits in the surface (figure 3(a-1)), whereas we could not find such structure in figure 3(b-1). In addition, the side-views of the samples are also given. Figure 3(a-2) is the side-view of Figure 3(a-1), which is observed from two directions (labelled red and green) vertical to each other, and Figure 3(b-2) is the side-view of Figure 3(b-1) with the same observation conditions. It can be seen in Figure 3(a-2) that the surface relief of the grating formed under condition A is close to sinusoidal, both in the direction labelled red and that labelled green. The vertical distances of two directions are approximately equal, being 115.63 nm in the red line direction and 123.22 nm in the green line direction. The grating pitches are 7.84 μm (red line direction) and 8.05 μm (green line direction). The difference of grating pitch along the two directions comes down to the incidence angles of pair L and pair K, which are not equal strictly. However, under condition B, as shown in Figure 3(b-2), the surface relief is one-dimensional.

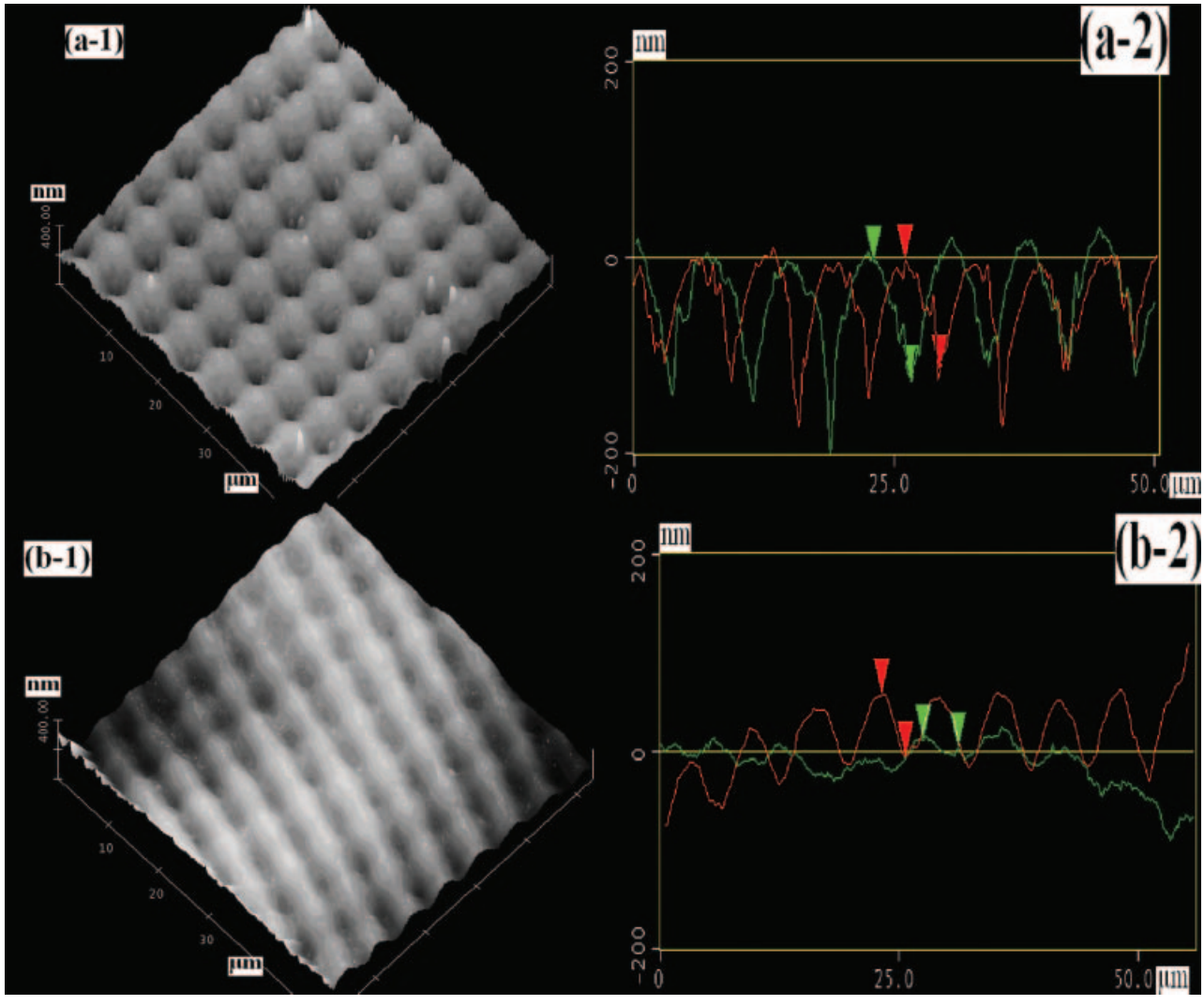

Figure 3. AFM morphologies of samples prepared under conditions $I_L/I_K=1:1$ (a-1, a-2) and $I_L/I_K=1:0.3$ (b-1, b-2). (a-1) and (b-1) are top views (a-2) and (b-2) are side-view analyses.

In that case, there is quite a difference between the vertical distance of the two directions, i.e. 64.25 nm and 6.64 nm.

To explain the morphology differences theoretically, 2D photopolymerisation dynamics model in section 3.2 is utilised. Using Equation (24), the monomer conversion (α) is simulated for the following parameter assumptions: the exposure intensity of every laser is equal and is $1.05\,\mathrm{mW\,cm^{-2}}$; $k_p/(k_t)^{0.5}=0.0008\,\mathrm{s^{-1}}$; σ_T is assumed as 0.8; $\Phi_S=0.005$; $\varepsilon(\lambda)=0.08\,\mu\mathrm{m^{-1}}$; $l=10\,\mu\mathrm{m}$; $x/\Lambda_x=y/\Lambda_y$, which vary from 0 to 5; t is the exposure time, in our experiment it was 1200 s. Thus, the monomer conversion under condition A ($I_L=I_K$) is shown in Figure 4(a); the conversions along x and y directions are equal, a result that reflects experimental observations. When I_L:I_K=1:0.3 (condition B), Equation (24) should be changed a little to

$$\alpha(x,y,t)=1-\exp\left\{-\frac{k_P}{\sqrt{k_t}}t\sqrt{\left[2I_x\left(1+\cos\frac{2\pi}{\Lambda_x}x\right)+2I_y\left(1+\cos\frac{2\pi}{\Lambda_y}y\right)\right]\sigma_T(1-10^{-\varepsilon(\Lambda)\Phi_s l})}\right\}. \quad (25)$$

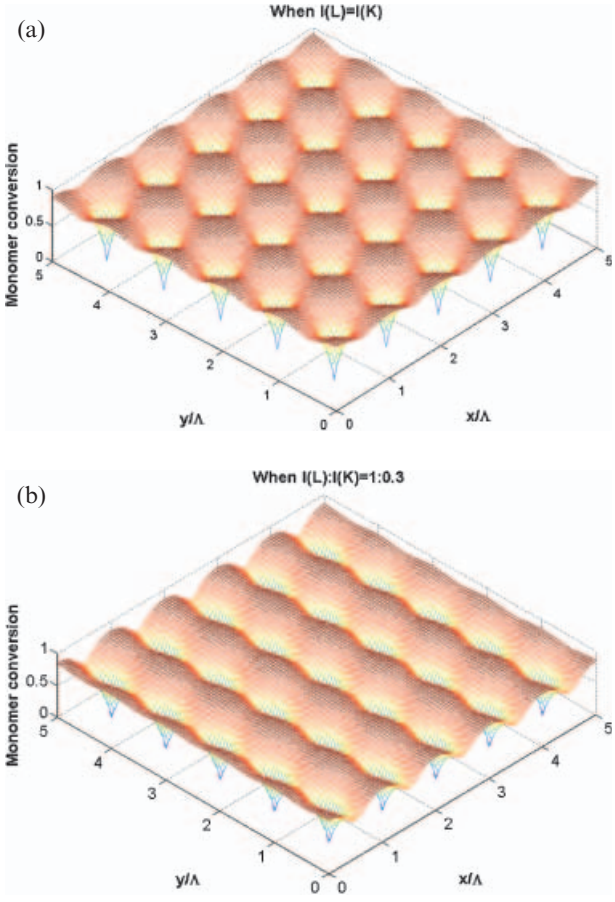

Figure 4. Theoretical simulations of monomer conversion under the assumption of $I_L=I_K$ (a) and I_L/I_K=1:0.3 (b).

The values of the parameters are fixed, and then simulated result of condition B is obtained. As shown in Figure 4(b), the monomer conversion is almost one-dimensional, which agrees very well with experimental results.

According to the results listed above, it is believed that the reason of the differences in the cases of condition A and B lies in the differences of photopolymerisation rate, which leads directly to the differences in chemical potential between interference fields caused by pair L and pair K. When the intensity ratio of pair L and pair K are large, the photopolymerisation rate of pair K is so small compared with pair L, then, the chemical potential between light and dark strips caused by pair K is weak, so the photopolymerisation and molecule diffusion will be overwhelmed by pair L, and a one-dimensional grating is formed. In contraat, when the ratio is close to each other, photopolymerisation equilibrium is constructed and chemical potentials caused by pair L and pair K is close and, thus, 2D gratings with better morphologies are formed.

Electro-optical properties

The E-O properties of the sample prepared under condition A were tested using the experimental setup described in section 2.2. The diffraction distributions for both the "OFF" state and the "ON" state are shown in Figure 5. The first-order diffraction intensities [$I(0,1)$, $I(0,-1)$, $I(1,0)$, $I(-1,0)$ labelled in Figure 5 a] at both states were determined; the results are presented in Table 1. As shown in Table 1, the intensities of four diffraction beams are approximately equal when there is no applied voltage, and the first-order diffraction efficiency is 36.6%. The first-order diffraction efficiency is defined as $\eta=(I_{0,1}+I_{0,-1}+I_{1,0}+I_{-1,0})/I_{in}$, where I_{in} is the total intensity of the incident beam. When there is an applied voltage on the sample, $12.5\,\mathrm{V\,\mu m^{-1}}$ in our experiments, the refractive indexes of the LC-rich zone and polymer-rich zone are almost equal, so refractive index modulation is very small and the diffraction beams disappear. The first-order diffraction efficiency obtained is only 3.5%.

Moreover, the diffraction distribution intensity is calculated with the model constructed in section 3.1. By using Equations (13)–(15), intensity distributions of "OFF" state and "ON" state can be simulated. The initiation value of the parameters contained in Equation (13) are as follows: the macroscopic length and width of the grating are $L_x=L_y=5$ mm, x and y are alterable parameters that vary from -0.4 mm to 0.4 mm and $z=10$ mm; λ is the test wavelength, which in our model is 0.6328 μm, corresponding

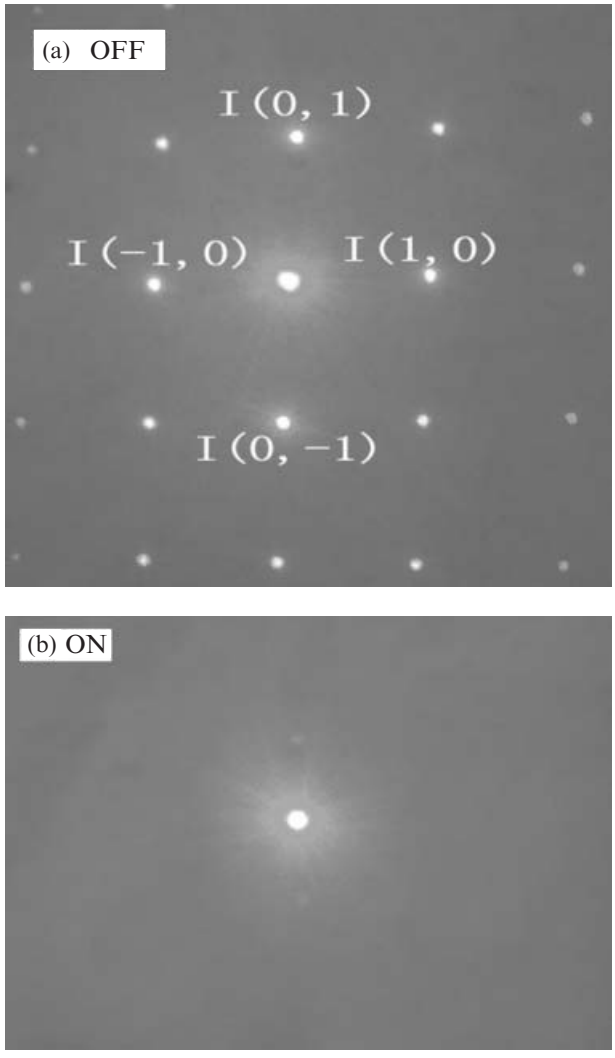

Figure 5. Diffraction pattern of 2-D electro-tunable grating in "OFF" state (a) and "ON" state (E=12.5 V μm^{-1}) (b), (other diffraction orders are present in the pictures).

to the He–Ne laser used in the experiments. For simplicity, let $\Lambda_x=\Lambda_y=8\,\mu m$. In our model, n_e and n_o in Equation (14) are 1.6925 and 1.5222, respectively, and the polymer refractive index, n_p, is 1.52. In our simulations, the refractive index of polymer-rich zone is assumed equal to that of the pure polymer. Such an assumption is not unreasonable. The reason is that, according to the theoretical conclusions of Meng *et al.* (*31*) and Kyu and Chiu (*32*), the LC concentration in the polymer-rich zone is less than 5%, thus when we calculated the refractive index of polymer-rich zone, it is unnecessary to consider LC

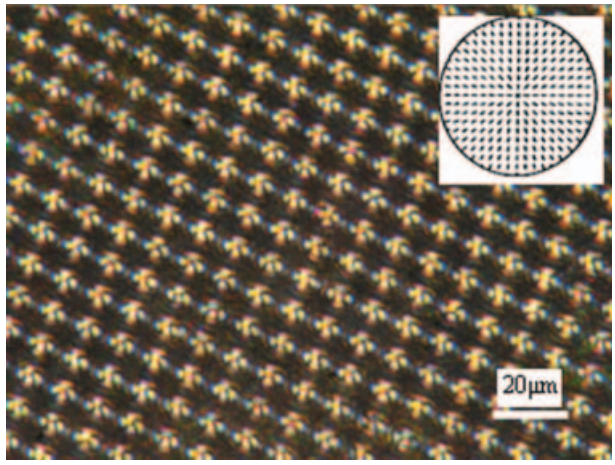

Figure 6. POM micrographs of samples prepared under conditions I_L/I_K=1:1, crossed polariser (1000×). Inset: schematic picture of the radial alignment of LC molecules in droplets.

trapped in the polymer. θ_0 in Equation (15) is usually 88°, the switch field of LC is $E_C=0.2\,V\,\mu m^{-1}$. B_2 is the refractive index modulation when there is an applied voltage of about 12.5 V μm^{-1} on the sample; through Equations (14)–(15), n_{LC} calculated is 1.5222, which is approximately equal to n_o, and B_2 is 0.1092, obtained by Equation (8b). In the case of no applied voltage, through POM with crossed polariser, it is convenient to study LC alignment in its droplet. As shown in Figure 6, many black-crosses are found on LC droplet. The reason is the radial alignment of LC molecules in droplets (*33, 34*). In radial droplets, the director everywhere is along the radial direction, as shown in the inset in of Figure 6. Thus the reflective index of LC should be averaged and it can be estimated

$$\bar{n}_{LC}=\sqrt{\left(2n_o^2+n_e^2\right)/3}. \tag{26}$$

In addition, it is estimated from the phase diagram of PDLC mixture reported in previous papers (*35, 36*) that there are about 15–20% polymer or monomer contained in LC droplets, theoretically, the so-called LC-rich zone. So the refractive index of the LC-rich zone should consider the polymer and the average refractive index should be expressed as

$$n_{LC-rich}=\sqrt{\phi_{LC}\bar{n}_{LC}^2+\phi_P n_P^2}, \tag{27}$$

where ϕ_P is estimated as 0.17 and ϕ_{LC} is 0.83.

Table 1. First-order diffraction intensity and efficiency tested by detector when in "OFF" state and "ON" state.

State	I(0,1)	I(0,−1)	I(1,0)	I(−1,0)	I_{1all}	I_{in}	$\eta=I_{1all}/I_{in}$
OFF (E=0)	0.066	0.059	0.067	0.071	0.263	0.718	36.6%
ON (E=12.5 V μm^{-1})	6×10^{-3}	6×10^{-3}	7×10^{-3}	6×10^{-3}	0.025	0.716	3.5%

Table 2. First-order diffraction intensity and efficiency of "OFF" state and "ON" state calculated through diffractive distribution model.

State	$I(0,1)$	$I(0,-1)$	$I(1,0)$	$I(-1,0)$	I_{1all}	I_{in}	$\eta=I_{1all}/I_{in}$
OFF ($E=0$)	0.1119	0.1119	0.1119	0.1119	0.4476	1	44.7%
ON ($E=12.5\,\mathrm{V\,\mu m^{-1}}$)	7.4×10^{-4}	7.4×10^{-4}	7.4×10^{-4}	7.4×10^{-4}	2.96×10^{-3}	1	0.3%

Then, the refractive index modulation B_2 in the case of no applied voltage is estimated as 2.3975.

According to values given above, the diffractive distribution of grating can be simulated through computer. The intensity of every order can be computed as

$$I(m,n)=J_m^2\left(\frac{B_2}{2}\right)J_N^2\left(\frac{B_2}{2}\right), \tag{28}$$

where m and n are Bessel orders.

Theoretical results for $I(0,1)$, $I(0,-1)$, $I(1,0)$, $I(-1,0)$ and η are given in Table 2. It is clear that when it is in the "OFF" state, the diffraction intensity of every beam is equal and the first-order diffraction efficiency is 44.7%. In contrast, for the "ON" state, the first-order beam efficiency is only 0.3%, close to zero.

There is a small discrepancy between the experimental and theoretical data. The reason might be the following. First, polymer contained in LC-rich zones might be more than 20%; it might be over 30% or more in actual samples (*37*). Because of this, $n_{\text{LC-rich}}$ decreases and, simultaneously, refractive index modulation also decreases, which leads to the first-order diffraction efficiency being smaller than theoretical results. Second, the diffraction intensity tested is the area-averaged result, whereas the theoretical result is the intensity at the centre point of every order, which might be larger than the average value.

To sum up, in order to improve E-O properties of the grating, materials and liquid crystals to form the grating must be index matching. In addition, to increase first-order diffraction efficiency, the optical anisotropy of the LCshould be large.

5. Conclusions

A single-step exposure setup for 2D electrically tuneable grating based on PDLC is proposed. 2D gratings with better E-O property and morphologies are obtained successfully. To improve the grating performance, some numerical simulations are presented. Through the analysis of experimental data and simulation results, it is confirmed that the intensity difference between the two pairs of beams has a significant effect on the morphology and the diffraction performance of the 2D grating. When the intensity of one pair is close to the other, the morphology and E-O property of grating are better. In addition, the refractive index modulation between polymer domain and LC domain is also important. With this understanding, we should select nematic liquid crystals with large Δn (n_e-n_o) to improve the efficiency of the 2D gratings. Finally, another important point is increasing the index matching between polymer and ordinary refractive index of LC.

Acknowledgements

This work was supported by the Natural Science Foundation (Grant Nos. 60578035 and 50473040) and Science Foundation of Jilin Province, China (Grant Nos. 20050520 and 20050321-2).

References

(1) Natarajan L.V.; Tondiglia V.P.; Sutherland R.L. *Chem. Mater.* **1993**, *5*, 1533–1538.
(2) Sutherland R.L.; Natarajan L.V.; Tondiglia V.P.; Bunning T.J.; Adams W.W. *Appl. Phys. Lett.* **1994**, *64*, 1074–1076.
(3) Tondiglia V.P.; Natarajan L.V.; Sutherland R.L.; Bunning T.J.; Adams W.W. *Opt. Lett.* **1995**, *20*, 1325–1327.
(4) Bunning T.J.; Natarajan L.V.; Tondiglia V.P.; Sutherland R.L.; Adams W.W. *Polymer* **1996**, *37*, 3147–3150.
(5) Roussel F.; Chan-Yu-King R.; Buisine J.M. *Eur. Phys. J. E* **2003**, *11*, 293–300.
(6) Tanaka K.; Kato K.; Tsuru S. *SID' 94 Dig.* **1994**, *25*, 37–40.
(7) Xianyu H.; Qi J.; Cohn R.F.; Crawford G.P. *Opt. Lett.* **2003**, *28*, 792–794.
(8) Sutherland R.L.; Natarajan L.V.; Tondiglia V.P.; Bunning T.J. *SPIE* **2003**, *5003*, 35–43.
(9) Domash L.H.; Chen Y.M.; Gozewski C.M.; Haugsjaa P.O.; Oren M. *SPIE* **1997**, *3010*, 214–228.
(10) Bowley C.C.; Crawford G.P. *Appl. Phys. Lett.* **1999**, *74*, 3096–3098.
(11) Bowley C.C.; Fontecchio A.K.; Crawford G.P. *Appl. Phys. Lett.* **2000**, *76*, 523–525.
(12) Massenot S.; Kaiser J.L.; Perez M.C.; Chevallier R. *Appl. Opt.* **2005**, *44*, 5273–5280.
(13) Wu S.T.; Fuh A.Y. *Jpn. J. Appl. Phys.* **2004**, *43*, 7077–7082.
(14) Liu Y.J.; Sun X.W.; Shum P.; Yin X.J. *Opt. Express* **2006**, *14*, 5634–5640.
(15) Liu Y.J.; Sun X.W. *Appl. Phys. Lett.* **2006**, *89*, 171101–171103.

(16) Rudhardt D.; Nieves A.F.; Link D.R. *Appl. Phys. Lett.* **2003**, *82*, 2610–2612.
(17) Kossyrev P.; Sousa M.E.; Crawford P.G. *Adv. Funct. Mater.* **2004**, *14*, 1227–1232.
(18) Gorkhali S.P.; Crawford G.P.; Qi J. *Mol. Cryst. liq. Cryst.* **2005**, *433*, 297–308.
(19) Jakubiak R.; Tondiglia V.P.; Natarajan L.V.; Sutherland R.L. *Adv. Mater.* **2005**, *17*, 2807–2811.
(20) Cai L.Z.; Feng C.S.; He M.Z.; Yang X.L.; Meng X.F.; Dong G.Y. *Opt. Express* **2005**, *13*, 4325–4330.
(21) Gorkhali S.P.; Qi J.; Crawford G.P. *Appl. Phys. Lett.* **2005**, *86*, 011110–011112.
(22) Lei M.; Yao B.; Rupp R.A. *Opt. Express* **2006**, *14*, 5803–5811.
(23) Sun X.H.; Tao X.M.; Xue P.; Szeto Y.S. *Appl. Phys. B* **2007**, *87*, 65–69.
(24) Sun X.H.; Tao X.M.; Xue P.; Szeto Y.S. *Appl. Phys. B* **2007**, *87*, 267–271.
(25) Ma J.; Liu Y.G.; Yu T.; Lu X.H.; Mu Q.Q.; Xuan L. *Chin. J. Liq. Cryst. Display* **2005**, *20*, 115–118.
(26) Born M.; Wolf E. *Principles of Optics*, 7th ed., Cambridge University Press: Cambridge, 1999.
(27) Sutherland R.L. *J. Opt. Soc. Am. B* **2002**, *19*, 2995–3003.
(28) Sutherland R.L.; Tondiglia V.P.; Natarajan L.V.; Bunning T.J. *J. appl. Phys.* **2004**, *96*, 951–965.
(29) Odian G. *Principles of Polymerization*; John Wiley & Sons: New York, 2004.
(30) Fernandez A.; Phillion D.W. *Appl. Opt.* **1998**, *37*, 473–478.
(31) Meng S.; Kyu T.; Natarajan L.V.; Tondiglia V.P.; Sutherland R.L.; Bunning T.J. *Macromolecules* **2005**, *38*, 4844–4854.
(32) Kyu T.; Chiu H.W. *Polymer* **2001**, *42*, 9173–9185.
(33) Doane J.W.; Waz N.A.; Wu B.G.; Zumer S. *Appl. Phys. Lett.* **1986**, *48*, 269–271.
(34) Wu S.T.; Yang D.K. *Reflective Liquid Crystal Displays*; John Wiley & Sons: New York, 2001.
(35) Shen C.; Kyu T. *J. chem. Phys.* **1995**, *102*, 556–562.
(36) Nwabunma D.; Kim K.J.; Lin Y.; Chien L.C.; Kyu T. *Macromolecules* **1998**, *31*, 6806–6812.
(37) Sutherland R.L.; Natarajan L.V.; Tondiglia V.P.; Chandra S.; Shepherd C.K.; Brandelik D.M.; Siwecki S.A. *J. Opt. Soc. Am. B* **2002**, *19*, 3004–3012.